ADVANCED FUNCTIONAL MATERIALS
www.afm-journal.de

# Scalable Nanowire Photonic Crystals: Molding the Light Emission of InGaN

*Yong-Ho Ra, Roksana Tonny Rashid, Xianhe Liu, Jaesoong Lee, and Zetian Mi**

**To date, there have been no efficient semiconductor light emitters operating in the green and amber wavelengths. This study reports on the synthesis of InGaN nanowire photonic crystals, including dot-in-nanowires, nanotriangles, and nanorectangles with precisely controlled size, spacing, and morphology, and further demonstrates that bottom-up InGaN photonic crystals can exhibit highly efficient and stable emission. The formation of stable and scalable band edge modes in defect-free InGaN nanowire photonic crystals is directly measured by cathodoluminescence studies. The luminescence emission, in terms of both the peak position ($\lambda \approx 505$ nm) and spectral linewidths (full-width-half-maximum ≈ 12 nm), remains virtually invariant in the temperature range of 5–300 K and under excitation densities of 29 W cm$^{-2}$ to 17.5 kW cm$^{-2}$. To the best of our knowledge, this is the first demonstration of the absence of Varshni and quantum-confined Stark effects in wurtzite InGaN light emitters—factors that contribute significantly to the efficiency droop and device instability under high-power operation. Such distinct emission properties of InGaN photonic crystals stem directly from the strong Purcell effect, due to efficient coupling of the spontaneous emission to the highly stable and scalable band-edge modes of InGaN photonic crystals, and are ideally suited for uncooled, high-efficiency light-emitting-diode operation.**

## 1. Introduction

Highly stable and efficient light-emitting devices are essentially required for a broad range of applications including lighting, display, communication, sensing, imaging, and medical diagnostics.[1–3] While GaN-based light emitting diodes (LEDs) exhibit efficient operation in the blue wavelength range, their efficiency and stability degrades considerably with increasing wavelengths, leading to the "green gap" in LED and laser technology.[4–9] The quantum efficiency ($\eta$) of a semiconductor light emitter is ultimately determined by

$$\eta \propto \frac{\tau_r^{-1}}{\tau_r^{-1} + \tau_{nr}^{-1}} \quad (1)$$

where $\tau_r$ and $\tau_{nr}$ represent the radiative and nonradiative lifetimes in the device active region, respectively. In conventional InGaN/GaN green and amber LEDs, the presence of large densities of defects and dislocations, due to the large lattice mismatch (≈11%) between InN and GaN, and Auger recombination, leads to a small $\tau_{nr}$ and therefore low quantum efficiency.[10–12] Moreover, the performance of conventional InGaN light emitters suffers severely from strain-induced polarization fields and the resulting quantum-confined Stark effect, which often results in a considerable blueshift in emission wavelengths (up to 30 nm) under high-power operation.[13,14] To date, a clear path to achieve efficient and stable semiconductor light emitters operating in the green, yellow, and amber wavelengths has remained elusive.[15,16]

Emission properties of a semiconductor light emitter are determined not only by the properties of the device active medium but also by the optical density of states surrounding the active region. For example, by exploiting the Purcell effect in an optical microcavity, the radiative lifetime ($\tau_r$) can be significantly reduced, thereby leading to enhanced internal quantum efficiency ($\eta$).[17] To date, however, there have been few demonstrations on the use of Purcell effect to bridge the "green gap" in semiconductor LEDs and lasers.[18–22] The Purcell factor, $F_p$, is determined by

$$F_p \propto \frac{Qg}{V} \quad (2)$$

where $Q$ is the quality factor, $V$ is the mode volume of the optical cavity, and $g$ is the mode degeneracy.[17] To enhance the Purcell factor, conventional design considerations are focused on small optical cavity size (on the order of micrometer),[23–26] whereas practical LED devices require extended optical mode spread over millimeter scale, i.e., three to six orders

Dr. Y. H. Ra, R. T. Rashid, X. Liu, Prof. Z. Mi
Department of Electrical and Computer Engineering
McGill University
3480 University Street, Montreal, Quebec H3A 0E9, Canada
E-mail: ztmi@umich.edu
X. Liu, Prof. Z. Mi
Department of Electrical Engineering and Computer Science
Center for Photonics and Multiscale Nanomaterials
University of Michigan
Ann Arbor, MI 48109, USA
Dr. J. S. Lee
Nano Electronics Lab
Samsung Advanced Institute of Technology
Suwon-si, Gyeonggi-do 443-803, South Korea

DOI: 10.1002/adfm.201702364

 

of magnitude larger than conventional designs. In addition, previously reported GaN optical cavities, including photonic crystals, are generally fabricated from epilayers using the top-down etching method, which inherently have large densities of defects and dislocations, with emission wavelengths limited to the blue and near-ultraviolet spectral range.[27–31]

In this work we show that such critical challenges can be addressed by using InGaN nanowire photonic crystals synthesized via the bottom-up method, wherein the formations of defects and dislocations are minimized due to the efficient surface strain relaxation. With the use of selective area epitaxy, we demonstrate that the size, spacing, and morphology of InGaN photonic crystals, including dot-in-nanowires, nanotriangles, and nanorectangles, can be precisely controlled, and, as such, spatially extended band edge modes can develop over a large area of such defect-free photonic crystals. It is further observed that InGaN photonic crystals exhibit remarkably stable emission, compared to conventional InGaN light emitters. The luminescence emission, in terms of both the peak position ($\lambda \approx 505$ nm) and spectral linewidths (full-width-half-maximum (FWHM) $\approx$ 12 nm), remained virtually invariant in the temperature range of 5–300 K and under excitation densities of 29 W cm$^{-2}$ to 17.5 kW cm$^{-2}$. To the best of our knowledge, this is the first demonstration of the absence of Varshni and quantum-confined Stark effects in wurtzite InGaN light emitters, factors that contribute significantly to the efficiency droop and device instability under high power operation. Such distinct emission properties of InGaN photonic crystals stem directly from the highly stable and scalable band edge modes, due to the precisely controlled size, position, and morphology of InGaN nanowire photonic crystals, and are ideally suited for uncooled, high-efficiency LED, and laser operation.

## 2. Results and Discussion

Photonic crystal nanostructures synthesized by the bottom-up method often exhibit non-negligible surface recombination as well as significant variations in size and morphology.[32–34] In this work, we show that these issues can be collectively addressed by selective-area epitaxy of GaN photonic crystals on nanopatterned substrate using plasma-assisted molecular beam epitaxy (MBE), wherein InGaN/AlGaN quantum dots are incorporated as the active medium to suppress surface recombination. Schematically shown in **Figure 1**a, a thin Ti layer was used as a growth mask on a GaN/sapphire substrate, and various nanoscale patterns were created on the Ti mask by e-beam lithography technique.[35–44] Each GaN photonic crystal, schematically shown in Figure 1b, consists of 400 nm *n*-GaN, ten vertically aligned InGaN/AlGaN quantum dots, and 80 nm *p*-GaN layer. Under selective area epitaxy conditions, Ga adatoms are only nucleated in the opening apertures, and no epitaxy takes place on the Ti mask. As such, the size and morphology of GaN photonic crystals are precisely determined by the opening apertures in the Ti mask. The incorporation of AlGaN barriers in active region, instead of GaN barriers, leads to the formation of an AlGaN shell surrounding the InGaN quantum dot active region, due to the smaller Al adatom migration length compared to Ga and In adatoms. The resulting core–shell like nanostructures, schematically shown in Figure 1b, can effectively suppress nonradiative surface recombination.[45,46]

The photoluminescence (PL) emission was measured using a 405 nm laser at room temperature. Shown in Figure 1b, it is seen that the photoluminescence intensity is enhanced by nearly a factor of eight, compared to InGaN/GaN nanostructures without the formation of AlGaN shell. Detailed structural characterization of the InGaN/AlGaN core–shell dot-in-nanowire structures is described elsewhere.[45–47] Shown in Figure 1c,d are the scanning electron microscope (SEM) images of InGaN/AlGaN hexagonal dot-in-nanowire, dot-in-nanotriangle, and dot-in-nanorectangle arrays, which exhibit straight sidewalls and uniform size distribution.[19] The photonic crystals can be arranged in various lattice structures, including rhombic and triangular lattices, with different orientations, illustrated in Figure 1c. Take the dot-in-nanowire array shown in Figure 1d as an example, the nanowire photonic crystals are arranged in a triangular lattice with a lattice constant of 250 nm. The nanowires have lateral sizes of 215 nm and length of 560 nm. The air gap between neighboring nanowires is 35 nm. The uniformity of InGaN nanowire photonic crystals across a large area is further shown in Figure S1 in the Supporting Information.

Significantly, InGaN/AlGaN dot-in-nanowire photonic crystals exhibit distinctly different emission characteristics, compared to conventional InGaN emitters. Shown in **Figure 2**a, strong emission was observed at 505 nm with a relatively narrow spectral linewidth of 12 nm for the photonic crystals illustrated in Figure 1d. The emission is highly uniform across a large nanowire photonic crystal structure (see Figure S2 in the Supporting Information). For comparison, conventional InGaN nanowire arrays or epilayers exhibit broad spectral linewidths (35–50 nm),[7,48–50] which are limited by the large inhomogeneous broadening associated with indium compositional variation and the presence of defects and strain field.[46,51] Variations of the light intensity versus excitation power are further shown in Figure 2b. The integrated luminescence intensity is nearly three times higher than InGaN/AlGaN dot-in-nanowire arrays grown under identical conditions but without the control of the nanowire spacing. The unique dependence of the luminescence emission on the nanowire spacing and height, as well as the impact of optical confinement of photonic crystals on the temperature and power-dependent emission characteristics of InGaN, is described next.

First, to understand the effect of optical confinement on the emission characteristics of InGaN, the photonic band structure of InGaN hexagonal nanowire arrays was calculated using the plane wave expansion method. Shown in **Figure 3**a,b, InGaN nanowires are arranged in a hexagonal lattice with a lattice constant $a$ and lateral dimension $d = 0.85a$, which is also shown in the structural characterization in Figure 1d. The refractive index of InGaN nanowires is 2.37. The normalized frequency of the band-edge mode is ≈0.49, which corresponds to $\lambda = 505$ nm for $a = 250$ nm. By adjusting the flat bands of leaky modes, e.g., frequencies around 0.49 to match the emission wavelengths of the active region, the luminescence efficiency can be significantly enhanced, due to the Purcell effect. The group velocity is determined by the slope of the dispersion curve in the photonic band structure. At the band edge, a low group velocity

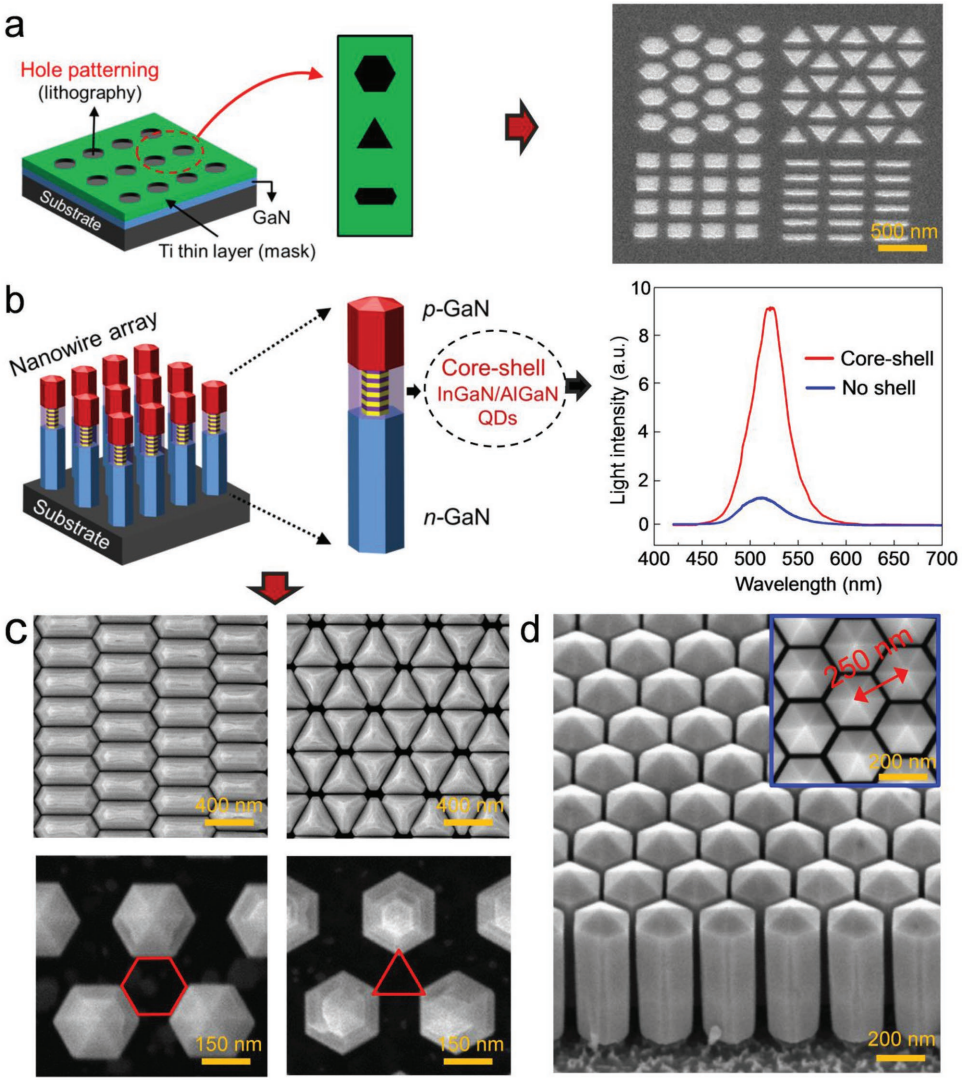


**Figure 1.** a) Schematic illustration of hole-patterned Ti thin film mask for the selective-area epitaxy of InGaN photonic crystals. SEM image of various nanoscale patterns formed on the Ti mask is shown in the right panel. b) Illustration of bottom-up InGaN/AlGaN core–shell dot-in-nanowire array grown on pattered substrate. Photoluminescence spectrum of InGaN/AlGaN core–shell dot-in-nanowires measured at room-temperature (red curve) is shown in the right panel. Also shown for comparison is the photoluminescence emission of InGaN/GaN dot-in-nanowires without AlGaN shell (blue curve). c) Top-view SEM images of InGaN/AlGaN hexagonal dot-in-nanowire, nanotriangle, and nanorectangle arrays. d) 45°-tilted-view SEM image of the nanowire photonic crystals arranged in a triangular lattice with a lattice constant of 250 nm. The top-view SEM image is shown in the inset.

is achieved, i.e., $dw/dk \rightarrow 0$ for frequencies around 0.49 near the Γ point, thereby leading to the formation of a stable and large cavity mode.[52] The low group velocity and the resulting long interaction time between radiation field and active material lead to a considerably enhanced spontaneous emission rate. Moreover, due to Bragg scattering, the light extraction efficiency will also be enhanced. Shown in Figure 3c is the electric field profile of the band edge mode calculated by the finite-element method for areal sizes of 5 × 5 μm. The calculated mode is TM polarized with electric field in parallel with the *c*-axis. Perfectly matched layer was used for the boundary condition, which can minimize any reflection at the simulation boundary.

The formation of stable and scalable optical modes in such bottom-up photonic crystals is further revealed by cathodoluminescence (CL) studies. Illustrated in Figure 3d is the cathodoluminescence image taken at 505 nm at room-temperature. The areal size being excited by the e-beam is 5 × 5 μm. It is seen that the band edge mode spreads across the entire photonic crystal structure, which is in excellent agreement with the calculation shown in Figure 3c. Strong light confinement occurs near the center region of nanowire arrays by the scattering of the band edge mode. Moreover, it is interesting to observe that strong photon confinement can also be achieved for photonic crystals with areal sizes as small as 2 × 2 μm and 1 × 1 μm, shown in Figure 3e,f, respectively, confirming the scalability of the band edge modes.[52] Detailed cathodoluminescence measurements were also performed for InGaN photonic crystals with different design parameters and at different emission wavelengths, shown in Figure S3 in the Supporting Information. These studies provided unambiguous evidence for the

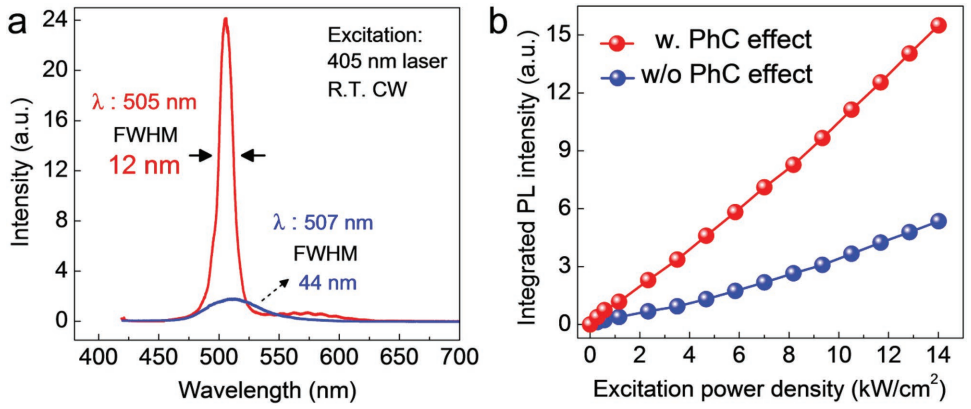


**Figure 2.** a) Photoluminescence spectrum of InGaN/AlGaN dot-in-nanowire photonic crystals measured at room-temperature (red curve). Also shown for comparison is the photoluminescence emission of conventional InGaN/AlGaN nanowires (blue curve) without controlled spacing. b) Variations of the light intensity versus excitation power density measured at room-temperature.

formation of strongly confined, highly uniform, and scalable band edge modes of InGaN photonic crystals, thereby offering a viable approach for realizing both small and large scale efficient light emitters.

We have further performed extensive studies of InGaN photonic crystals with different design parameters. Shown in Figure 3g are variations of the luminescence intensity and spectral linewidth with nanowire spacing while keeping *a* constant. Epitaxy conditions were optimized to have similar spontaneous emission from the quantum dot active regions when the nanowire spacing is varied. It is seen that the emission characteristics, in terms of both the spectral linewidth and integrated intensity, depend critically on the nanowire spacing. The highest luminescence intensity and narrowest spectral linewidth occurs for a nanowire spacing of 35 nm. A decrease, or increase in nanowire spacing, leads to a reduction in the luminescence

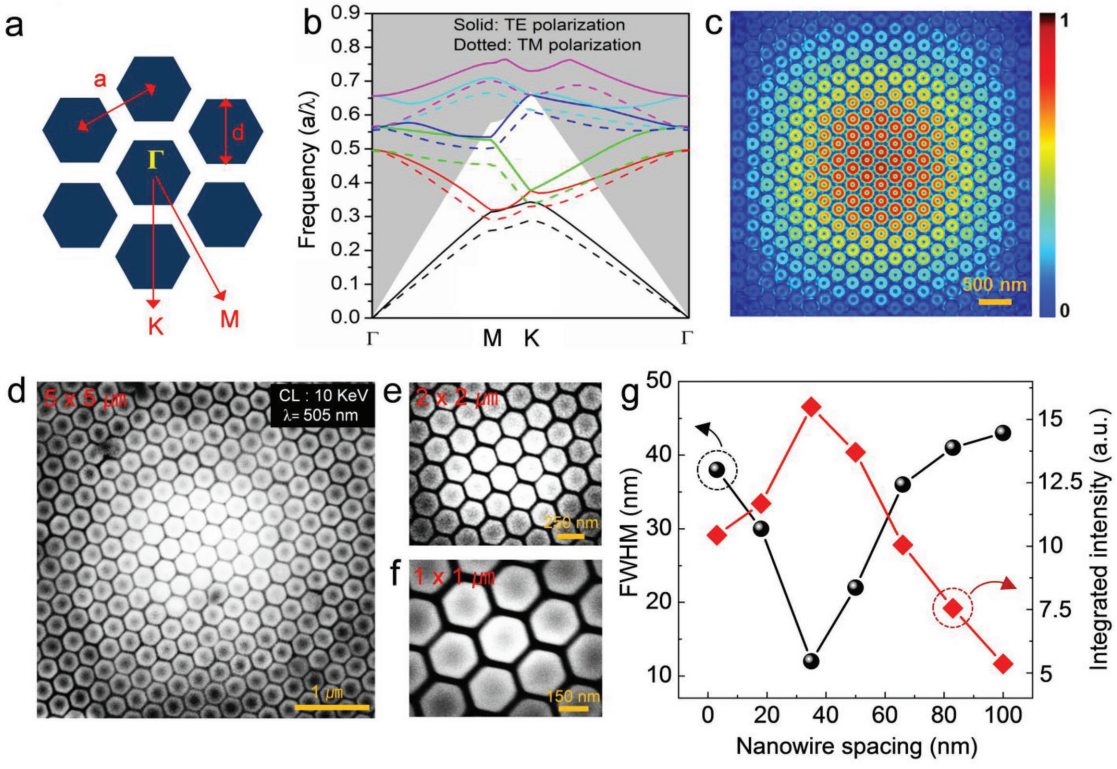


**Figure 3.** a) Schematic diagram of the simulated photonic crystals, including the lattice constant *a*, nanowire lateral size *d*, and the reciprocal lattice vectors. b) Calculated photonic band structure of the 2D hexagonal array of nanowires (the corresponding SEM is shown in Figure 1d). c) The electric field profile of the band edge mode calculated by the 3D finite-difference time-domain method for a bands-edge mode ($\lambda = 505$ nm). d) Cathodoluminescence mapping image of an areal size of $5 \times 5$ μm$^2$ measured at a wavelength of 505 nm. Cathodoluminescence mapping images over e) $2 \times 2$ μm and f) $1 \times 1$ μm regions, respectively. g) Variations of the integrated luminescence intensity and FWHM of InGaN photonic crystals versus nanowire spacing.

intensity, accompanied by a significant increase in the spectral linewidth, which suggests a reduced or minimal level of coupling between the quantum dot spontaneous emission and the band edge mode. Since the light extraction efficiency of leaky modes does not change significantly for such small variations of nanowire spacing,[17,53] the measured variations of luminescence emission may be primarily attributed to the change of the Purcell effect. Based on the measured internal quantum efficiency of 20–30% at room-temperature for the InGaN photonic crystals and assuming a constant light extraction efficiency, the magnitude of Purcell enhancement factor ($F_p$) is estimated to be in the range of 3 for the spatially extended band edge mode, which is comparable to that for the very small mode in a nanocavity.[19] The relatively large Purcell factor is partly related to the large mode degeneracy factor $g$ shown in Equation (2) associated with the large modal volume.[17] The extreme sensitivity of the Purcell effect on the nanowire spacing (radius), compared to the conventional slab photonic crystals,[17,53] is partly related to the quasi 3D nature of InGaN nanowire photonic crystals, due to the presence of planar GaN substrate as well as the finite length of InGaN nanowires. This observation is further supported by the critical dependence of the emission characteristics of InGaN nanowire photonic crystals on the height of nanowires (see in Figure S4 of the Supporting Information).

Due to the presence of quantum-confined Stark effect, conventional InGaN light emitters generally exhibit significant blueshift with increasing pumping power.[54–56] Moreover, the emission characteristics also vary considerably with temperature, due to the Varshni's effect. By contrast, we have measured remarkably stable emission characteristics for InGaN nanowire photonic crystals. Shown in **Figure 4**a are the normalized photoluminescence emission spectra of InGaN photonic

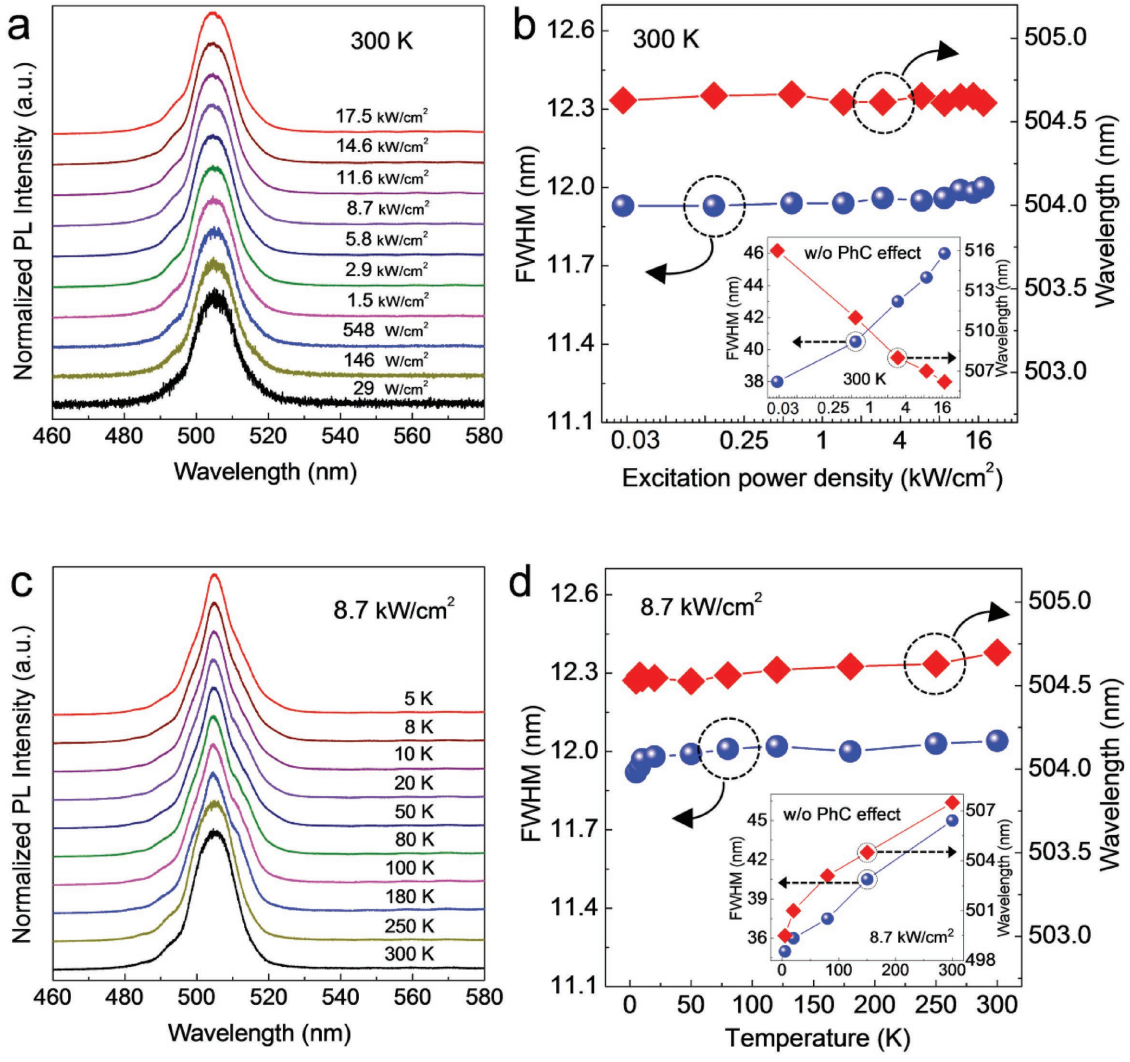


**Figure 4.** a) Photoluminescence emission spectra of InGaN photonic crystals measured at excitation power from 29 W cm$^{-2}$ to 17.5 kW cm$^{-2}$ at room-temperature. b) Variations of the emission peak and spectral linewidth versus excitation power in the InGaN photonic crystal. Inset: variations of the emission peak and spectral linewidth in conventional InGaN nanowire arrays without the photonic-crystal effect. c) Photoluminescence emission spectra of InGaN photonic crystals measured in the temperature range of 5–300 K under 8.7 kW cm$^{-2}$ continuous-wave pumping conditions. d) Variations of the emission peak and spectral linewidth versus temperature in the InGaN photonic crystal. Inset: variations of the emission peak and spectral linewidth in the conventional InGaN nanowire arrays without photonic-crystal effect.

crystals measured at excitation power from 29 W cm$^{-2}$ to 17.5 kW cm$^{-2}$ at room temperature. It is seen that the emission spectra remain nearly identical. Shown in Figure 4b, the peak emission wavelengths (≈505 nm) and spectral linewidths (FWHM ≈ 12 nm) are virtually invariant versus pumping power. Luminescence emission spectra of InGaN dot-in-nanowire photonic crystals measured in the temperature range of 5–300 K are further shown in Figure 4c, which was measured under 8.7 kW cm$^{-2}$ continuous wave pumping condition. Figure 4d shows variations of the emission peak and spectral linewidth versus temperature. It is seen that both the emission wavelengths (≈505 nm) and spectral linewidths (≈12 nm) remained nearly constant in the temperature range of 5–300 K. For comparison, conventional InGaN nanowire arrays without photonic crystal effect exhibit significant variations in the photoluminescence emission properties with increasing temperature and pumping power, shown in the insets of Figure 4b,d. The remarkably stable emission characteristics of InGaN photonic crystals stem directly from the efficient coupling of InGaN quantum dot emission to the robust band edge modes of InGaN photonic crystals, which is virtually independent of device operating conditions and largely determines the emission characteristics.

## 3. Conclusions

In summary, we have demonstrated the bottom-up synthesis of InGaN nanowire photonic crystals with precisely controlled size, spacing, and morphology, which can serve as the fundamental building blocks of a new generation of photonic crystal devices and systems. By coupling the light emission into the band edge mode of InGaN photonic crystals, significantly enhanced emission efficiency and reduced spectral broadening was measured. Moreover, the luminescence emission exhibits remarkable stability: there are virtually no variations in the emission characteristics, in terms of both the emission peak and spectral linewidth in the temperature range of 5–300 K and for pumping power variations from 29 W cm$^{-2}$ to 17.5 kW cm$^{-2}$. To our knowledge, this is the first demonstration of the absence of quantum-confined Stark effect and Varshni's effect in InGaN light emitters. These unique characteristics, together with the scalable band edge optical mode,[57] high light-extraction efficiency,[58] on-demand beam characteristics,[59,60] and full-color emission,[36,39,61] render bottom-up GaN nanowire photonic crystals well suited for ultrahigh-efficiency, large-area LED and laser devices, as well as integrated nanophotonic circuits in the ultraviolet and visible spectral range.

## 4. Experimental Section

*Ti-Mask-Patterned Substrate*: A 10 nm Ti layer was used as the mask layer for selective area growth, which was deposited on GaN (4 μm)/$Al_2O_3$ (0001) substrate by e-beam evaporator system. Subsequently, a poly(methyl methacrylate) layer was selectively exposed by e-beam lithography. Thereafter, the exposed Ti thin film area was etched using reactive dry-etching technique. The nanohole patterned substrate was cleaned by hydrogen chloride prior to loading into the MBE growth chamber.

*Molecular Beam Epitaxial Growth*: The bottom-up InGaN/AlGaN nanowire heterostructures were fabricated using radio frequency plasma-assisted MBE. The growth process included a surface nitridation of the Ti mask layer for 10 min at 400 °C. The growth conditions for Si-doped GaN nanowires included a growth temperature of 800 °C, with a nitrogen flow rate of 0.6 standard cubic centimeter per minute, a forward plasma power of 350 W, and Ga beam equivalent pressure (BEP) of $3.5 \times 10^{-7}$ Torr. In order to introduce the formation of the AlGaN shell structure in the active region, the InGaN dot with a thickness of ≈3 nm is first grown at the center region of GaN nanowire. Due to the strain induced self-organization, the size of the InGaN dot becomes smaller than the GaN nanowire diameter. The incorporation of AlGaN barriers, instead of GaN barriers, leads to the formation of an AlGaN shell surrounding the InGaN quantum dot active region, due to the smaller Al adatom migration length compared to Ga and In adatoms.[45,47] As a consequence, the entire growth front including the top and sidewalls of the InGaN core region can be covered by AlGaN layer, thereby leading to the spontaneous formation of Al-rich large band-gap shell structures.[62] Growth conditions for the InGaN/AlGaN quantum dot active region included a substrate temperature of ≈600 °C, Ga BEP of $9 \times 10^{-9}$ Torr, in BEP of $7.5 \times 10^{-8}$ Torr and Al BEP of $4.5 \times 10^{-9}$ Torr. By repeating this process, vertically aligned InGaN/AlGaN multiquantum dot layers can be formed with highly uniform AlGaN shell structure surrounding the active region. Growth conditions for the Mg-doped GaN layer included a Ga BEP of $3.5 \times 10^{-7}$ Torr and Mg BEP of $2 \times 10^{-9}$ Torr with substrate temperature of 750 °C.

*PL Measurement*: A 405 nm laser was used as the excitation source for the PL measurement of the InGaN/AlGaN nanowire heterostructures. A visible neutral density filter was used to adjust the laser excitation powers in range of 29 W cm$^{-2}$–17.5 kW cm$^{-2}$. The emitted light was spectrally resolved by a high-resolution spectrometer, and was detected by a high sensitivity and low noise liquid nitrogen cooled CCD in the visible range. Temperature-dependent PL measurements were carried out using a helium closed-loop cryostat.

*CL Measurement*: CL measurement was performed using a Zeiss Supra 55 VP field emission gun SEM equipped with a cryogenic stage coupled to a Gatan MonoCL 2 setup. A gold thin film layer was deposited on the substrate in order to suppress charging effect induced by the electron beam. The accelerating voltage used in the CL characterization is 10 keV. The emission was collected by a parabolic mirror and detected using a dry-ice cooled photomultiplier tube.

## Supporting Information

Supporting Information is available from the Wiley Online Library or from the author.

## Acknowledgements

Y.H.R. and R.T.R. contributed equally to this work. This work was supported by Samsung Corporation, University of Michigan, and the Natural Sciences and Engineering Research Council of Canada (NSERC).

## Conflict of Interest

The authors declare no conflict of interest.

## Keywords

gallium nitride, light emitting diodes, nanowires, photonic crystals, selective area epitaxy

Received: May 3, 2017
Revised: June 27, 2017
Published online: August 4, 2017

[1] W. Huang, J. M. Li, L. M. Yang, Z. L. Jin, Z. G. Zhong, Y. Liu, Q. Y. Chou, F. Li, *Opt. Laser Technol.* **2011**, *43*, 214.
[2] E. F. Schubert, J. K. Kim, *Science* **2005**, *308*, 1274.
[3] M. K. Choi, J. Yang, K. Kang, D. C. Kim, C. Choi, C. Park, S. J. Kim, S. I. Chae, T. H. Kim, J. H. Kim, T. Hyeon, D. H. Kim, *Nat. Commun.* **2015**, *6*, 7149.
[4] T. Honda, T. Kobayashi, S. Egawa, M. Sawada, K. Sugimoto, T. Baba, *J. Cryst. Growth* **2007**, *298*, 736.
[5] H. P. Nguyen, K. Cui, S. Zhang, S. Fathololoumi, Z. Mi, *Nanotechnology* **2011**, *22*, 445202.
[6] S. M. Sadaf, Y. H. Ra, H. P. Nguyen, M. Djavid, Z. Mi, *Nano Lett.* **2015**, *15*, 6696.
[7] Y. Jiang, Y. Li, Y. Li, Z. Deng, T. Lu, Z. Ma, P. Zuo, L. Dai, L. Wang, H. Jia, W. Wang, J. Zhou, W. Liu, H. Chen, *Sci. Rep.* **2015**, *5*, 10883.
[8] Y. T. Lin, T. W. Yeh, Y. Nakajima, P. D. Dapkus, *Adv. Funct. Mater.* **2014**, *24*, 3162.
[9] T. Langer, A. Kruse, F. A. Ketzer, A. Schwiegel, L. Hoffmann, H. Jonen, H. Bremers, U. Rossow, A. Hangleiter, *Phys. Status Solidi C* **2011**, *8*, 2170.
[10] Y. C. Shen, G. O. Mueller, S. Watanabe, N. F. Gardner, A. Munkholm, M. R. Krames, *Appl. Phys. Lett.* **2007**, *91*, 141101.
[11] E. Kioupakis, P. Rinke, K. T. Delaney, C. G. Van de Walle, *Appl. Phys. Lett.* **2011**, *98*, 161107.
[12] K. T. Delaney, P. Rinke, C. G. Van de Walle, *Appl. Phys. Lett.* **2009**, *94*, 191109.
[13] C.-F. Huang, C.-Y. Chen, C.-F. Lu, C. C. Yang, *Appl. Phys. Lett.* **2007**, *91*, 051121.
[14] M. Strassburg, A. Hoffmann, J. Holst, J. Christen, T. Riemann, F. Bertram, P. Fischer, *Phys. Status Solidi C* **2003**, *0*, 1835.
[15] Y. L. Chang, J. L. Wang, F. Li, Z. Mi, *Appl. Phys. Lett.* **2010**, *96*, 013106.
[16] C. Balasubramanian, V. P. Godbole, V. K. Rohatgi, A. K. Das, S. V. Bhoraskar, *Nanotechnology* **2004**, *15*, 370.
[17] M. Boroditsky, R. Vrijen, T. F. Krauss, R. Coccioli, R. Bhat, E. Yablonovitch, *J. Lightwave Technol.* **1999**, *17*, 2096.
[18] S. Ishizawa, K. Kishino, R. Araki, A. Kikuchi, S. Sugimoto, *Appl. Phys. Express* **2011**, *4*, 055001.
[19] A. C. Scofield, S. H. Kim, J. N. Shapiro, A. Lin, B. Liang, A. Scherer, D. L. Huffaker, *Nano Lett.* **2011**, *11*, 5387.
[20] T. Kouno, K. Kishino, K. Yamano, A. Kikuchi, *Opt. Express* **2009**, *17*, 20440.
[21] L. M. Chang, C. H. Hou, Y. C. Ting, C. C. Chen, C. L. Hsu, J. Y. Chang, C. C. Lee, G. T. Chen, J. I. Chyi, *Appl. Phys. Lett.* **2006**, *89*, 071116.
[22] Y. J. Lu, J. Kim, H. Y. Chen, C. Wu, N. Dabidian, C. E. Sanders, C. Y. Wang, M. Y. Lu, B. H. Li, X. Qiu, W. H. Chang, L. J. Chen, G. Shvets, C. K. Shih, S. Gwo, *Science* **2012**, *337*, 450.
[23] O. Painter, R. K. Lee, A. Scherer, A. Yariv, J. D. O'Brien, P. D. Dapkus, I. I. Kim, *Science* **1999**, *284*, 1819.
[24] H. G. Park, S. H. Kim, S. H. Kwon, Y. G. Ju, J. K. Yang, J. H. Baek, S. B. Kim, Y. H. Lee, *Science* **2004**, *305*, 1444.
[25] Y. J. Lu, C. Y. Wang, J. Kim, H. Y. Chen, M. Y. Lu, Y. C. Chen, W. H. Chang, L. J. Chen, M. I. Stockman, C. K. Shih, S. Gwo, *Nano Lett.* **2014**, *14*, 4381.
[26] T. C. Lu, S. W. Chen, T. T. Kao, T. W. Liu, *Appl. Phys. Lett.* **2008**, *93*, 111111.
[27] J. B. Wright, S. Liu, G. T. Wang, Q. Li, A. Benz, D. D. Koleske, P. Lu, H. Xu, L. Lester, T. S. Luk, I. Brener, G. Subramania, *Sci. Rep.* **2013**, *3*, 2982.
[28] D. U. Kim, S. Kim, J. Lee, S. R. Jeon, H. Jeon, *IEEE Photonics Techol. Lett.* **2011**, *23*, 1454.
[29] H. Matsubara, S. Yoshimoto, H. Saito, Y. Jianglin, Y. Tanaka, S. Noda, *Science* **2008**, *319*, 445.
[30] Q. Li, K. R. Westlake, M. H. Crawford, S. R. Lee, D. D. Koleske, J. J. Figiel, K. C. Cross, S. Fathololoumi, Z. Mi, G. T. Wang, *Opt. Express* **2011**, *19*, 25528.
[31] J. B. Wright, S. Campione, S. Liu, J. A. Martinez, H. Xu, T. S. Luk, Q. Li, G. T. Wang, B. S. Swartzentruber, L. F. Lester, I. Brener, *Appl. Phys. Lett.* **2014**, *104*, 041107.
[32] S. Zhao, H. P. T. Nguyen, M. G. Kibria, Z. Mi, *Prog. Quantum Electron.* **2015**, *44*, 14.
[33] K. H. Li, X. Liu, Q. Wang, S. Zhao, Z. Mi, *Nat. Nanotechnol.* **2015**, *10*, 140.
[34] H. J. Joyce, Q. Gao, H. Hoe Tan, C. Jagadish, Y. Kim, J. Zou, L. M. Smith, H. E. Jackson, J. M. Yarrison-Rice, P. Parkinson, M. B. Johnston, *Prog. Quantum Electron.* **2011**, *35*, 23.
[35] K. Kishino, H. Sekiguchia, A. Kikuchi, *J. Cryst. Growth* **2009**, *311*, 2063.
[36] Y. H. Ra, R. Wang, S. Y. Woo, M. Djavid, S. M. Sadaf, J. Lee, G. A. Botton, Z. Mi, *Nano Lett.* **2016**, *16*, 4608.
[37] S. D. Hersee, X. Sun, X. Wang, *Nano Lett.* **2006**, *6*, 1808.
[38] K. Kishino, S. Ishizawa, *Nanotechnology* **2015**, *26*, 225602.
[39] R. Wang, Y. H. Ra, Y. P. Wu, S. Zhao, H. P. T. Nguyen, I. Shih, Z. Mi, *Proc. SPIE* **2016**, *9748*, 97481S.
[40] S. Albert, A. Bengoechea-Encabo, M. A. Sanchez-Garcia, X. Kong, A. Trampert, E. Calleja, *Nanotechnology* **2013**, *24*, 175303.
[41] Z. Gacevic, D. Gomez Sanchez, E. Calleja, *Nano Lett.* **2015**, *15*, 1117.
[42] K. A. Bertness, A. W. Sanders, D. M. Rourke, T. E. Harvey, A. Roshko, J. B. Schlager, N. A. Sanford, *Adv. Funct. Mater.* **2010**, *20*, 2911.
[43] S. C. Lee, B. Pattada, S. D. Hersee, Y. B. Jiang, S. R. J. Brueck, *IEEE J. Quantum Electron.* **2005**, *41*, 596.
[44] G. M. Yang, M. H. Macdougal, P. D. Dapkus, *Electron. Lett.* **1995**, *31*, 886.
[45] H. P. Nguyen, M. Djavid, S. Y. Woo, X. Liu, A. T. Connie, S. Sadaf, Q. Wang, G. A. Botton, I. Shih, Z. Mi, *Sci. Rep.* **2015**, *5*, 7744.
[46] H. P. Nguyen, S. Zhang, A. T. Connie, M. G. Kibria, Q. Wang, I. Shih, Z. Mi, *Nano Lett.* **2013**, *13*, 5437.
[47] R. J. Wang, X. D. Liu, I. Shih, Z. T. Mi, *Appl. Phys. Lett.* **2015**, *106*, 261104.
[48] J. S. Son, Y. Honda, H. Amano, *Opt. Express* **2014**, *22*, 3585.
[49] J. L. Liu, J. L. Zhang, G. X. Wang, C. L. Mo, L. Q. Xu, J. Ding, Z. J. Quan, X. L. Wang, S. Pan, C. D. Zheng, X. M. Wu, W. Q. Fang, F. Y. Jiang, *Chin. Phys. B* **2015**, *24*, 067804.
[50] S. F. Li, A. Waag, *J. Appl. Phys.* **2012**, *111*, 071101.
[51] H. P. Nguyen, S. Zhang, K. Cui, X. Han, S. Fathololoumi, M. Couillard, G. A. Botton, Z. Mi, *Nano Lett.* **2011**, *11*, 1919.
[52] R. Merlin, S. M. Young, *Opt. Express* **2014**, *22*, 18579.
[53] R. K. Lee, Y. Xu, A. Yariv, *J. Opt. Soc. Am. B* **2000**, *17*, 1438.
[54] N. G. Young, R. M. Farrell, S. Oh, M. Cantore, F. Wu, S. Nakamura, S. P. DenBaars, C. Weisbuch, J. S. Speck, *Appl. Phys. Lett.* **2016**, *108*, 061105.
[55] Y. Ji, W. Liu, T. Erdem, R. Chen, S. Tiam Tan, Z.-H. Zhang, Z. Ju, X. Zhang, H. Sun, X. Wei Sun, Y. Zhao, S. P. DenBaars, S. Nakamura, H. Volkan Demir, *Appl. Phys. Lett.* **2014**, *104*, 143506.
[56] M. A. Reshchikov, H. Morkoc, *J. Appl. Phys.* **2005**, *97*, 061301.
[57] J. J. Wierer, A. David, M. M. Megens, *Nat. Photonics* **2009**, *3*, 163.
[58] C. Wiesmann, K. Bergenek, N. Linder, U. T. Schwarz, *Laser Photonics Rev.* **2009**, *3*, 262.
[59] S. Iwahashi, Y. Kurosaka, K. Sakai, K. Kitamura, N. Takayama, S. Noda, *Opt. Express* **2011**, *19*, 11963.
[60] S. Noda, M. Yokoyama, M. Imada, A. Chutinan, M. Mochizuki, *Science* **2001**, *293*, 1123.
[61] H. Sekiguchi, K. Kishino, A. Kikuchi, *Appl. Phys. Lett.* **2010**, *96*, 231104.
[62] S. M. Sadaf, S. Zhao, Y. Wu, Y. H. Ra, X. Liu, S. Vanka, Z. Mi, *Nano Lett.* **2017**, *17*, 1212.

 